Available online at www.sciencedirect.com
SCIENCE DIRECT®
ELSEVIER
Optics Communications 229 (2004) 253–261
OPTICS COMMUNICATIONS
www.elsevier.com/locate/optcom

Theoretically predicted performance and frequency-scaling rule of a Symmetric-Mach-Zehnder optical 3R gating

Yoshiyasu Ueno *

Graduate School of Electronic Engineering, University of Electro-Communications, 1-5-1 Chofugaoka, Chofu, Tokyo 182-8585, Japan

Received 30 July 2003; received in revised form 13 November 2003; accepted 19 November 2003

Abstract

The performance of an optical 3R gating with a Symmetric-Mach-Zehnder semiconductor gate is predicted from our gating model and a set of realistic component-parameter values. In particular, the trade-off between amplitude-noise suppression and pattern-induced internal noise is demonstrated with an assumed 40-Gb/s input signal. Furthermore, a frequency-scaling rule for the 3R gate is analytically predicted that takes into account the optimum carrier lifetime and the carrier-injection level for the semiconductor-optical amplifiers inside the gate. The predicted scaling rule was numerically confirmed through our simulation, where a signal bit-rate of 160 Gb/s was assumed.

PACS: 42.79.Sz; 42.79.Hp; 42.70.Nq; 42.65.Wi

Keywords: All-optical; 3R; Regeneration; Semiconductor optical amplifier; Interference; Jitter tolerence; Scaling rule; Gating; OTDM

1. Introduction

All-optical Symmetric-Mach-Zehnder (SMZ) semiconductor gates [1–3] are expected to be useful for optical 3R gating [4–9] at ultrahigh bit-rates; i.e., 40–160 Gb/s and even beyond 160 Gb/s. In fact, SMZ 3R gates that include semiconductor optical amplifiers (SOAs) offer high tolerance with respect to input timing, as has been experimentally observed [6,7,9]. The amplitude noise in optical signals has also been all-optically suppressed (i.e., without EO conversion) in experiments [4,5,7]. However, this author is unaware of any theoretical model accounting for such 3R performance.

For accelerating the 3R gating speed from 80 Gb/s [5,6] to 160 Gb/s or higher, the carrier lifetime of SOAs or new materials is widely recognized to be the most important component or material parameter. SOA research [10,11] and more fundamental materials research [12–14] have taken several directions. Both the optimum carrier lifetime and the optimum carrier-injection level for the SOAs inside such 3R gates, however, are thought to strongly depend on the signal frequency (the bit-rate). Because these dependences have not

* Corresponding author. Tel./fax: +81424435807.
E-mail address: y.ueno@ieee.org (Y. Ueno).

0030-4018/$ - see front matter
doi:10.1016/j.optcom.2003.11.043

been clearly modeled, they have not been taken into account in the on-going SOA or materials research to the best of this author's knowledge. If a frequency-scaling rule could be derived from a well-established 3R-gating model, such a rule would offer a clearer roadmap for use in SOA and materials research.

In this work, the outlines of the above two aspects of 3R gating performance are numerically predicted based on our original gating model and a set of realistic SOA parameter values. In particular, the tradeoff between amplitude-noise suppression and the pattern-induced internal noise, which is an inherent property of this type of 3R gate, is demonstrated. Furthermore, a frequency-scaling rule is analytically predicted from the theoretical model. The predicted rule was numerically confirmed through our simulation.

2. The theoretical model

An optical 3R gating with an all-optical SMZ gate was assumed (Fig. 1); this form of gating has been experimentally studied elsewhere [4,8]. The time-dependent amplitude of the pseudo-random input data signal pulses to the SMZ gate was assumed to be

$$E_{\mathrm{signal}}^{\mathrm{input}}(t) = \sum_m C_m E_{\mathrm{signal}} \operatorname{sech}\left(\frac{t - T_m}{T_{\mathrm{w}}}\right), \quad m = 1, 2, \ldots, \infty, \tag{1}$$

where the digital code C_m is either 0 or 1. The pattern length of the pseudo-random digital sequence C_m was set to 2^{15}–1. T_m is the pulse position in time and T_{w} is the pulse-width parameter. The full-width at half-maximum (T_{FWHM}) of a sech pulse is related to T_{w} as

$$T_{\mathrm{FWHM}} = 2\log\left(1 + \sqrt{2}\right) T_{\mathrm{w}}. \tag{2}$$

Inside the SMZ gate, the input signal pulses were split into two identical components. One of these components then reached the first SOA (SOA1) in Fig. 1 as

$$E_{\mathrm{signal}}^{\mathrm{SOA1}}(t) = E_{\mathrm{signal}}^{\mathrm{input}}(t). \tag{3}$$

The second component was given a specific delay time, Δt, before arriving at the second SOA (SOA2) as

$$E_{\mathrm{signal}}^{\mathrm{SOA2}}(t) = E_{\mathrm{signal}}^{\mathrm{input}}(t + \Delta t). \tag{4}$$

The amplitude of the input clock pulses to the two SOAs was

$$E_{\mathrm{clock}}(t) = \sum_m E_{\mathrm{clock}} \operatorname{sech}\left(\frac{t - T_{\mathrm{clock}} - T_m}{T_{\mathrm{w}}}\right), \quad m = 1, 2, \ldots, \infty, \tag{5}$$

where T_{clock} is a parameter for adjusting the clock's input timing with respect to the signal.

When SOA1 receives $E_{\mathrm{signal}}^{\mathrm{SOA1}}(t)$ and $E_{\mathrm{clock}}(t)$, the excess carrier density $\overline{n_{\mathrm{c}}(t)}$ inside SOA1 is assumed to be governed by the following rate equation [15,16]:

$$\frac{\mathrm{d}}{\mathrm{d}t}\overline{n_{\mathrm{c}}^{\mathrm{SOA1}}(t)} = \frac{I_{\mathrm{op}}}{qV} - \frac{\overline{n_{\mathrm{c}}^{\mathrm{SOA1}}(t)}}{\tau_{\mathrm{c}}} - \frac{1}{V}\left(G\left\{\overline{n_{\mathrm{c}}^{\mathrm{SOA1}}(t)}\right\} - 1\right) \times \frac{\left|E_{\mathrm{clock}}(t)\right|^2 + \left|E_{\mathrm{signal}}^{\mathrm{SOA1}}(t)\right|^2}{\hbar\omega}. \tag{6}$$

In a similar manner, the density inside SOA2 is assumed to be

$$\frac{\mathrm{d}}{\mathrm{d}t}\overline{n_{\mathrm{c}}^{\mathrm{SOA2}}(t)} = \frac{I_{\mathrm{op}}}{qV} - \frac{\overline{n_{\mathrm{c}}^{\mathrm{SOA2}}(t)}}{\tau_{\mathrm{c}}} - \frac{1}{V}\left(G\left\{\overline{n_{\mathrm{c}}^{\mathrm{SOA2}}(t)}\right\} - 1\right) \times \frac{\left|E_{\mathrm{clock}}(t)\right|^2 + \left|E_{\mathrm{signal}}^{\mathrm{SOA2}}(t)\right|^2}{\hbar\omega}. \tag{7}$$

The excess carrier density in each SOA, $\overline{n_{\mathrm{c}}(t)}$, in this work is defined as

$$\overline{n_{\mathrm{c}}(t)} \equiv \frac{1}{L}\int_{z=0}^{L} n_{\mathrm{c}}(z,t)\,\mathrm{d}z = \frac{1}{L}\int_{z=0}^{L} \{n(z,t) - n_{\mathrm{tr}}\}\,\mathrm{d}z. \tag{8}$$

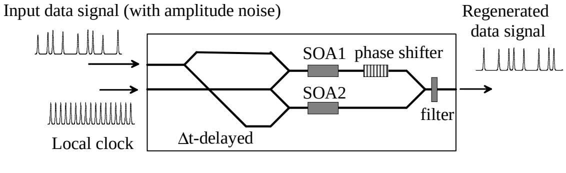

Fig. 1. Optical 3R gating with an all-optical SMZ gate.

In Eqs. (6)–(8), I_{op} is the injection current, q is the elementary charge, τ_c is the carrier lifetime, and n_{tr} is the transparency carrier density. L and V are, respectively, the length and the volume of the SOA active layer, $\hbar$ is Planck's constant, and ω is the optical angular frequency of the optical pulses. $n(z,t)$ is the carrier density at a position z inside the SOA at time t. The temporal chip gain of each SOA was assumed to be

$$G(t) \equiv \exp\left[\mathrm{d}g/\mathrm{d}n_c\,\overline{n_c(t)}\,\Gamma L\right], \tag{9}$$

where $\mathrm{d}g/\mathrm{d}n_c$ is the differential gain and Γ is the optical confinement factor.

At the output of SOA1 and SOA2, the respective clock pulses were assumed to be expressed as

$$E_{\mathrm{clock}}^{\mathrm{SOA1}}(t) = \sqrt{G\left\{\overline{n_c^{\mathrm{SOA1}}(t)}\right\}}\exp\left[\mathrm{i}\Phi\left\{\overline{n_c^{\mathrm{SOA1}}(t)}\right\}\right]E_{\mathrm{clock}}(t), \tag{10}$$

and

$$E_{\mathrm{clock}}^{\mathrm{SOA2}}(t) = \sqrt{G\left\{\overline{n_c^{\mathrm{SOA2}}(t)}\right\}}\exp\left[\mathrm{i}\Phi\left\{\overline{n_c^{\mathrm{SOA2}}(t)}\right\}\right]E_{\mathrm{clock}}(t). \tag{11}$$

While the $\sqrt{G\{\overline{n_c(t)}\}}$ factor in Eqs. (10) and (11) governs the cross-gain modulation, the $\exp\lfloor \mathrm{i}\Phi\{\overline{n_c^{\mathrm{SOA2}}(t)}\}\rfloor$ factor governs the cross-phase modulation. The non-linear phase shift $\Phi\{\overline{n_c(t)}\}$, which the respective clock pulses receive after propagating through the respective SOAs, was assumed to be linearly proportional to the excess carrier density

$$\Phi(t) = -k_0\,\mathrm{d}n_r/\mathrm{d}n_c\,\overline{n_c(t)}\,\Gamma L, \tag{12}$$

where k_0 is the wave number in vacuum and $\mathrm{d}n_r/\mathrm{d}n_c$ is the non-linear change in the refractive index.

The regenerated signal pulses are generated when the two clock pulses $E_{\mathrm{clock}}^{\mathrm{SOA1}}(t)$ and $E_{\mathrm{clock}}^{\mathrm{SOA2}}(t)$ are optically combined with each other at the output of the Mach-Zehnder interferometer. The regenerated signal pulses are therefore written as

$$E_{\mathrm{signal}}^{\mathrm{output}}(t) = \left\{E_{\mathrm{clock}}^{\mathrm{SOA1}}(t) + \exp(\mathrm{i}\Delta\Phi_b)\,E_{\mathrm{clock}}^{\mathrm{SOA2}}(t)\right\}/2, \tag{13}$$

where $\Delta\Phi_b$ is the interferometer's phase bias. The interferometer's phase bias is adjusted with the phase shifter (bias-phase shifter) shown in Fig. 1.

Note that for simplicity the basic equations used here contain only the lowest-order terms. For instance, both the SOAs' material gain in Eq. (9) and the non-linear refractive-index change in Eq. (12) were assumed to be only linearly proportional to the excess carrier density. The feasibility of these assumptions has been experimentally verified through several types of gating experiments [15,16].

3. The parameter values

The parameter values assumed in this work are summarized in Tables 1 and 2. In Table 2, G_0 is the nominal unsaturated gain of a typical SOA inside the 3R gates. G_0 is generally defined as the small-signal gain when the excess carrier density $\overline{n_c(t)}$ inside the SOA reaches an equilibrium value $\overline{n_c^0}$ with a nominal current injection I_{op}^0

$$G_0 = G\left(\overline{n_c} = \overline{n_c^0}\right). \tag{14}$$

Because every part of an SOA, including the facet reflectivity, is designed using G_0 and $\overline{n_c^0}$, other parameters in this work – P_{sat}, $\Delta\Phi_{max}$, and τ_c – were based on values previously measured in the vicinity of $\overline{n_c} = \overline{n_c^0}$ with I_{op}^0 [15,16]. The maximum phase shift $\Delta\Phi_{max}$ is defined as

$$\begin{aligned}\Delta\Phi_{max} &\equiv \Phi\left(\overline{n_c} = \overline{n_c^0}\right) - \Phi(\overline{n_c} = 0)\\ &= k_0\,\mathrm{d}n_r/\mathrm{d}n_c\,\overline{n_c^0}\,\Gamma L.\end{aligned} \tag{15}$$

The $\overline{n_c^0}$ in Eq. (15) is related to P_{sat} and G_0

$$\overline{n_c^0} = \frac{1}{V}\frac{P_{sat}\ln G_0}{\hbar\omega}. \tag{16}$$

Table 1
Input pulse parameters

Description	Value (42 Gb/s)	Value (168 Gb/s)
Signal pulse width	2.0 ps	0.50 ps
Signal pulse energy	100 fJ	100 fJ
Signal power	+3.2 dBm	+9.2 dBm
Pseudo-random word length	2^{15}–1	2^{15}–1
Clock pulse width	2.0 ps	0.50 ps
Clock pulse energy	800 fJ	800 fJ

Table 2
Gate parameters

Parameter	Description	Value (42 Gb/s)	Value (168 Gb/s)
G_0	Unsaturated gain	28 dB	28 dB
P_{sat}	Gain saturation energy	180 fJ	180 fJ
$\Delta\Phi_{max}$	Phase shift at complete carrier depletion, $\Delta\Phi(\Delta n_c = n_c^0)$	+2.0π	+2.0π
τ_c	Carrier lifetime	50.0 ps	12.5 ps
I_{op}^0	Nominal injection current	150 mA	600 mA
I_{op}	Enhanced current injection	440 mA	1700 mA
I_{op}^{enh}	Injection enhancement factor	2.9	2.9
Δt	Delay time for the interference	11.9 ps	2.98 ps
$\Delta\Phi_b$	Interferometer phase bias	1.060π	1.060π

The nominal injection current, however, is generally insufficient for 3R gating, because the relatively strong clock pulses that are introduced to suppress the signal-pattern-induced effects consequently deplete the peak carrier density. The injection current (I_{op}) in this work is therefore assumed to be increased from I_{op}^0 by a specific factor (I_{op}^{enh}), as shown in Table 2. Note that the temporal gain $G(t)$ never goes above the nominal unsaturated gain G_0 even after the injection enhancement given in Table 2. Nor does the excess carrier density $\overline{n_c(t)}$ ever rise above the equilibrium value $\overline{n_c^0}$. This is because the injection enhancement is introduced only to compensate for the carrier depletion. We believe that all of the parameter values for the 42-Gb/s gating in Tables 1 and 2 are realistic with respect to those previously reported (e.g. [15,16]).

The unsaturated gain G_0 and the gain saturation energy P_{sat} for the clock pulses were, respectively, assumed to be equal to those for the input data pulses (Table 2). Consequently, a possible difference between the SOA gains for the input data and clock pulses in the previous experimental works is neglected in this work.

4. Amplitude-noise suppression

Fig. 2 shows a typical pair of calculated 42-Gb/s signal waveforms. The pulse width was assumed to be 2.0 ps so that a relatively large tolerance to the input timing could be obtained. The delay time, Δt, for the input signal pulse to the second SOA was set to half of the pulse distance (11.9 ps). An

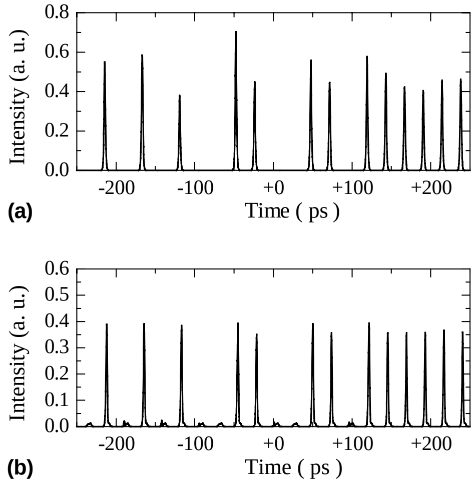

Fig. 2. Calculated 42-Gb/s pseudo-random signal waveforms: (a) before the 3R gate and (b) after the 3R gate.

random noise in the normal distribution was added to the electric field amplitude of each '1' pulse in the input signal in Fig. 2(a), so that the Q^2 value of its eye diagram dropped to 16.4 dB. (The random noise was added independently from the pseudo-random input bit pattern.) The output waveform in Fig. 2(b) demonstrated that the amplitude noise was dramatically suppressed after the 3R gating.

Fig. 3 shows the noise-suppression property in the eye diagram. Fig. 3(c) and (d) corresponds to the results from Fig. 2(a) and (b), respectively. Even when we further increased the noise in the input signal (Fig. 3(e)), the output eye diagram was only slightly degraded (Fig. 3(f)).

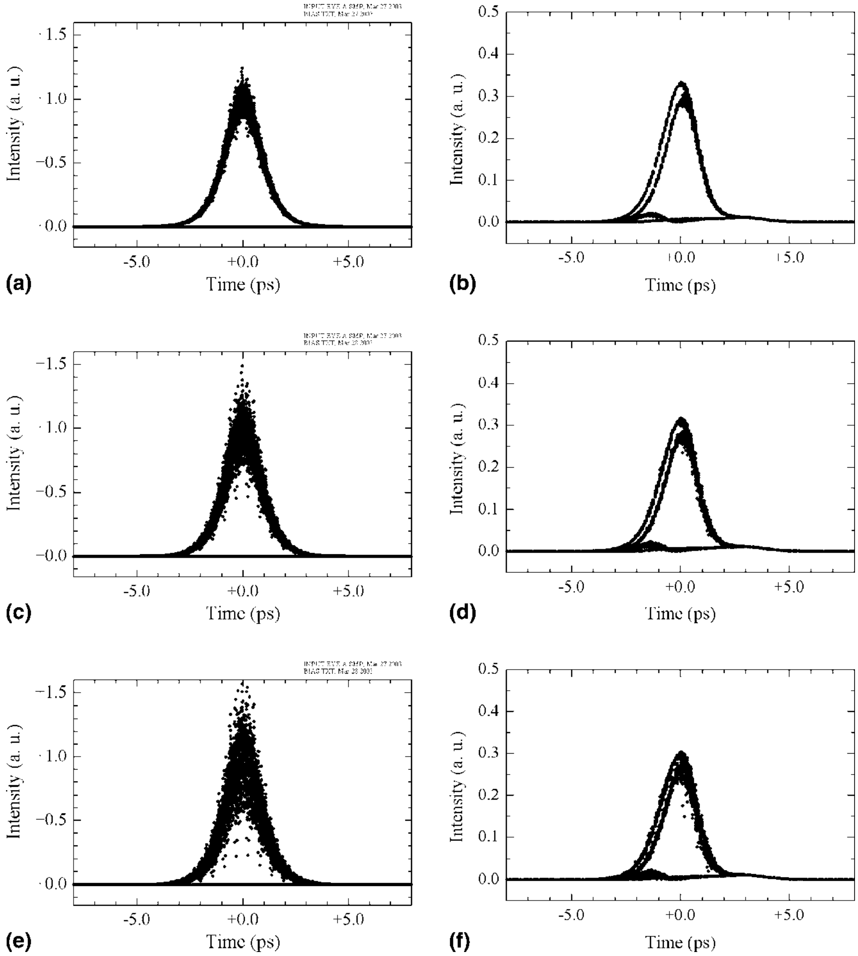

Fig. 3. Calculated 42-Gb/s eye diagrams: (a), (c) and (e) before the 3R gate; (b), (d) and (f) after the 3R gate. The Q^2 values at the 3R input were set to 22.4 dB (a), 16.4 dB (b), and 12.8 dB (c).

Fig. 4 shows another noise-suppression property taken from more systematically calculated eye diagrams. In this work, the Q factor of the input and output random data signals were defined as

$$Q = \frac{a_1 - a_0}{\sigma_1}, \tag{17}$$

where a_1 and a_0 are the mean values of the 1-bit and 0-bit intensity levels, respectively, at time T_{peak} when the average 1-bit pulse waveform reaches its maximum. σ_1 is the standard deviation of the 1-bit intensity level at T_{peak}.

The solid curve in Fig. 4 indicates the Q^2 value of output eye diagrams, including those in Fig. 3, as a function of the Q^2 value of the respective input

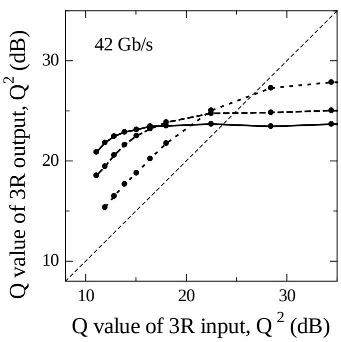

Fig. 4. Trade-off between noise suppression and pattern-induced noise. The input signal-pulse energies were assumed to be 50.0 (solid curve), 12.5 (dashed curve), and 3.13 fJ/pulse (dotted curve).

eye diagram. In this example, the output Q^2 value remained above 24 dB even when the input Q^2 value fell to below 16 dB. The solid curve also indicates that the output Q^2 value saturates even when the input Q^2 value is increased to above 26 dB. This saturation level is attributed to the so-called pattern-induced noise from the gate itself. In fact, most of the noise seen in Fig. 3(b) is attributed to pattern-induced noise.

When the averaged input pulse energy was decreased by a factor of either 4 (dashed curve in Fig. 4) or 16 (dotted curve in Fig. 4), the pattern-induced noise was improved. However, the noise-suppression performance was clearly reduced. This was attributed to the decrease in the non-linear phase shift with the input pulse energy. Thus, the input pulse energy to the 3R gate should be optimized while taking into account the tradeoff between the noise-suppression performance and the pattern-induced noise in this type of optical 3R gating.

5. Tolerance to the input timing

The input timing of each signal in Figs. 2–4 was adjusted so that each clock pulse coincided with the center of each gate window formed by the two-split signal pulses. Fig. 5 shows calculated eye diagrams where we slightly delayed the input-signal timing (ΔT_{IN}) by either −2.4 or +1.2 ps with respect to the window's center. The input signals were assumed to contain the same amplitude noise as that in Fig. 3(b). As shown in Fig. 5, the quality of the output eye diagram was reasonably tolerant with respect to the input timing offset ΔT_{IN} from −2.4 to +1.2 ps. The calculated output Q^2 values were 26.8 dB ($\Delta T_{IN} = -2.4$ ps, Fig. 5(a)), 24.6 dB ($\Delta T_{IN} = 0$ ps, Fig. 5(b)), and 23.8 dB ($\Delta T_{IN} = +1.2$ ps, Fig. 5(c)), respectively. (According to the definition in Eq. (17), the small amounts of noise in the '0' bits in Fig. 5(b) and (c) were ignored.)

The calculated output Q value is shown in Fig. 6 as a function of the input timing offset ΔT_{IN}. The output eye diagrams were approximately acceptable inside both timing region A (-6.0 ps $< \Delta T_{IN} < +1.6$ ps) and B (-15.9 ps $< \Delta T_{IN} < -9.2$ ps). In case of the timing regime A, in view of the optical phase difference between the two-split clock components before interference, the data pulses to SOA1 (Fig. 1) generated the output '1' pulses. In case of the regime B in contrast, the data pulses to SOA2 contributed more to the generation of output '1' pulses than those to SOA1. The amount of noise in the '1'-bit pulses was unacceptable in most of the regions outside regions A and B. The noise in the '0'-bit time slots (as was only slightly seen in Fig. 5) was particularly unacceptable inside a narrow timing region where -7.5 ps $< \Delta T_{IN} < -6.0$ ps. As indicated by the dashed curve in Fig. 6, the peak-to-peak intensity

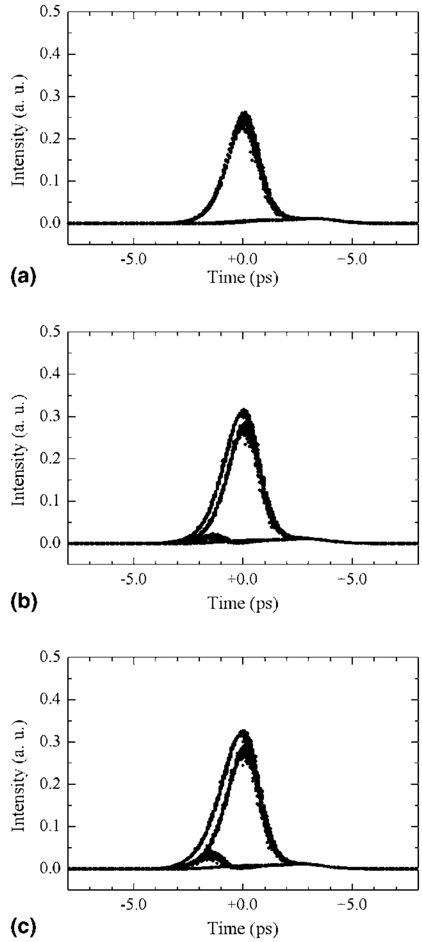

Fig. 5. Calculated 42-Gb/s eye diagrams after the 3R gate. The input signals were assumed to be delayed by −2.4 ps (a), ±0 ps (b), and +1.2 ps (c), with respect to the input clock. The Q^2 value at the 3R input was set to 16.4 dB.

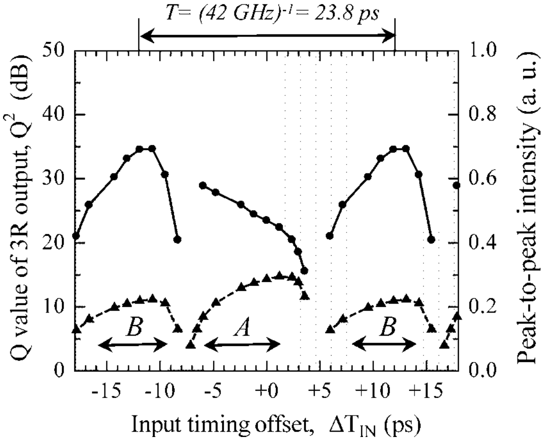

Fig. 6. Calculated tolerance of the 3R gating with respect to input timing. (solid curve) The Q^2 value of the output pulses. (dashed curve) The averaged peak-to-peak intensity of the output pulses. The assumed input Q^2 value was 16.4 dB. The quality of the output eye diagram was reasonably acceptable when the input timing was inside the two timing regions A and B. The logic of the output signal was non-inverted throughout these two timing regions.

of the output signal also turned out to be slightly dependent on the input timing.

Finally, it should be emphasized that the output logic in both regions A and B was non-inverted. Thus, Figs. 5 and 6 demonstrate the tolerance of the 3R gating with respect to the signal's input timing.

6. Frequency-scaling rule for 3R gating

We have found that we can quadruple, for example, the frequency of any type of 3R gating result when we scale the input and gate parameters given in Tables 1 and 2. This is done as follows: (1) the widths of the signal and clock pulses are narrowed by a factor of 4, (2) the energies of the signal and clock pulses are maintained, (3) the carrier lifetime of the two SOAs is shortened by a factor of 4, (4) the carrier injection is increased by a factor of 4, (5) the injection enhancement factor is maintained, and (6) the interferometer delay time Δt is shortened by a factor of 4. The parameter values for 168-Gb/s gating in Tables 1 and 2 were obtained according to this frequency-scaling rule.

Of items (1)–(6), items (1), (3), and (6) had intuitively been expected. In contrast, items (2), (4), and (5) were unexpected by this author. The frequency-scaling rule given above was theoretically derived in this work as follows. We assumed a specific carrier-density evolution $n_c(t)$ fulfills a rate equation that is simplified from Eq. (6)

$$\frac{d}{dt}n_c(t) = J - \frac{n_c(t)}{\tau_c} - (G\{n_c(t)\} - 1)\,n_p f_p, \qquad (18)$$

where J is the current-injection term, n_p is the total photon number of the input pulses, and f_p is the frequency of the input pulses. After Eq. (18), we have found that the four-times faster carrier evolution $n'_c(t) \equiv n_c(4t)$ fulfills the following rate equation:

$$\frac{d}{dt}n'_c(t) = J' - \frac{n'_c(t)}{\tau'_c} - \left(G\{n'_c(t)\} - 1\right) n'_p f'_p, \qquad (19)$$

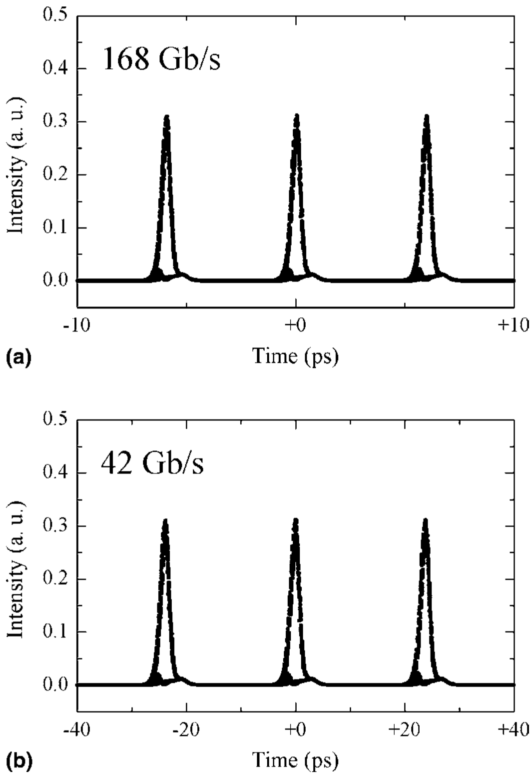

Fig. 7. Output eye diagrams: (a) with a 168-Gb/s input signal and the frequency-scaled parameters from Tables 1 and 2; (b) with a 42-Gb/s input signal, for comparison. The assumed input Q^2 value was 16.4 dB.

when the parameters are scaled as $\tau_c' \equiv \tau_c/4$, $f_p' \equiv 4f_p$, and $J' \equiv 4J$. Eq. (19) indicates that the frequency-scaled carrier-density evolution $n_c'(t)$ will be generated from these scaled parameters. It is thus theoretically derived that frequency-scaled output waveforms are generated with these scaled input pulses and gate parameters.

To confirm this frequency-scaling rule, we calculated the 3R gating with a 168-Gb/s data signal using the frequency-scaled parameters from Tables 1 and 2. The calculated eye diagram of the 168-Gb/s regenerated data signal is shown in Fig. 7(a). For comparison, that with a 42-Gb/s data signal is shown in Fig. 7(b). The input Q^2 value was assumed to be 16.4 dB for both calculations. A comparison of Fig. 7(a) and (b) shows that the 3R gating result was precisely frequency-scaled from 42 to 168-Gb/s. Thus, the frequency-scaling rule given above was successfully confirmed through this numerical simulation.

7. Conclusion

The performance of optical 3R gating with a SMZ semiconductor gate was predicted from a numerical simulation using an original gating model and a set of realistic component-parameter values. In particular, the inherent trade-off relationship between the noise-suppression performance and the pattern-induced internal noise of this type of 3R gating was modeled, apparently for the first time. The magnitude of this gate's tolerance with respect to input timing was also numerically estimated. It turned out that the timing-tolerance window is split into two regions. The output logic was non-inverted throughout the two timing-tolerance windows.

After the successful modeling of the SMZ 3R gating, we analytically derived a frequency-scaling rule from intentionally simplified model equations, and then confirmed its validity through a numerical simulation. The scaling rule has indicated that we should be able to quadruple the maximum bitrate for the 3R gate by: (1) reducing the SOA's carrier lifetime by a factor of 4 and (2) increasing the carrier-injection level by a factor of 4. The typical optimum carrier lifetime for 160-Gb/s 3R gating in our results was 12 ps, while that for 40-Gb/s gating was 50 ps. The frequency-scaling rule predicted in this work should be helpful for on-going research into both SOAs and materials, and thus should help accelerate the gating speed to above 160 Gb/s.

Acknowledgements

The author acknowledges the financial support of NEC Corporation from November 2002 to March 2003.

References

[1] K. Tajima, Jpn. J. Appl. Phys. 32 (1993) L1746.
[2] K. Tajima, S. Nakamura, Y. Sugimoto, Appl. Phys. Lett. 67 (1995) 3709.
[3] N.S. Patel, K.A. Rauschenbach, K.L. Hall, IEEE Photon. Technol. Lett. 8 (1996) 1695.
[4] L. Billes, J.C. Simon, B. Kowalski, M. Henry, G. Michaud, P. Lamouler, F. Alard, in: The Technical Digest of the 23rd European Conference on Optical Communications (ECOC'97), Edinburgh, Scotland, September 22–25, 1997, vol. 2, p. 269.
[5] A.E. Kelly, I.D. Phillips, R.J. Manning, A.D. Ellis, D. Nesset, D.G. Moodie, R. Kashyap, Electron. Lett. 35 (1999) 1477.
[6] Y. Ueno, S. Nakamura, K. Tajima, IEEE Photon. Technol. Lett. 13 (2001) 469.
[7] Y. Ueno, S. Nakamura, J. Sasaki, T. Shimoda, A. Furukawa, T. Tamanuki, T. Sasaki, K. Tajima, in: The Technical Digest of the 27th European Conference on Optical Communications (ECOC'2001), Amsterdam, The Netherlands, September 30–October 4, 2001, paper Th.F.2.1.
[8] B. Dagens, A. Labrousse, R. Brenot, B. Lavigne, M. Renaud, in: The Digest of the Optical Fiber Communication Conferrence (OFC'2003), vol. 2, Atlanta, USA, March 23–28, 2003, paper ThX1.
[9] M. Tsurusawa, K. Nishimura, R. Inohara, M. Usami, in: The Digest of the Optical Fiber Communication Conference (OFC'2003), vol. 2, Atlanta, USA, March 23–28, 2003, paper ThX3.
[10] M. Tsurusawa, K. Nishimura, M. Usami, Jpn. J. Appl. Phys. 1 41 (2002) 1199.
[11] T.P. Hessler, M.-A. Dupertuis, B. Deveaud, J.-Y. Emery, B. Dagens, Appl. Phys. Lett. 81 (2002) 3119.

[12] T. Akiyama, N. Georgiev, T. Mozume, H. Yoshida, A.V. Gopal, O. Wada, Electron. Lett. 37 (2001) 129.
[13] N. Iizuka, K. Kaneko, N. Suzuki, Appl. Phys. Lett. 77 (2000) 648.
[14] I. Waki, C. Kumtornkittikul, Y. Shimogaki, Y. Nakano, in: Technical Digest of the 10th International Workshop on Festosecond Technology (FST'2003), Makuhari, Japan, July 16–17, 2003, paper WB-2.
[15] Y. Ueno, S. Nakamura, K. Tajima, Opt. Lett. 23 (1998) 1846.
[16] Y. Ueno, S. Nakamura, K. Tajima, J. Opt. Soc. Am. B 19 (2002) 2573.